Assessing Linear Control Strategies for Zero-Speed Fin Roll Damping

Available online at www.sciencedirect.com

ScienceDirect

IFAC Papers Online CONFERENCE PAPER ARCHIVE

IFAC PapersOnLine 59-22 (2025) 776–781

Assessing Linear Control Strategies for Zero-Speed Fin Roll Damping

Nikita Savin [*,**] **Elena Ambrosovskaya** [*,**] **Dmitry Romaev** [*]
Anton Proskurnikov [***]

[*] *Navis JSC, St. Petersburg, Russia*
[**] *St. Petersburg Electrotechnical University "LETI", Russia*
[***] *Politecnico di Torino, Italy*

Abstract: Roll stabilization is a critical aspect of ship motion control, particularly for vessels operating in low-speed or zero-speed conditions, where traditional hydrodynamic fins lose their effectiveness. In this paper, we consider a roll damping system, developed by Navis JSC, based on two actively controlled zero-speed fins. Unlike conventional fin stabilizers, zero-speed fins employ a drag-based mechanism and active oscillations to generate stabilizing forces even when the vessel is stationary. We propose a simple linear control architecture that, however, accounts for nonlinear drag forces and actuator limitations. Simulation results on a high-fidelity vessel model used for HIL testing demonstrate the effectiveness of the proposed approach.

Keywords: Roll damping, zero-speed fin stabilizers, ship motion control, stability

1. INTRODUCTION

Roll damping is a well-studied problem in ship motion control, crucial for passenger comfort and vital for cargo safety, efficiency, and precision tasks on commercial and specialized vessels. A wide range of anti-roll methods exists, from passive bilge keels and tuned tanks to active stabilizers; see, e.g., (Perez and Blanke, 2012; Perez, 2006).

Rudder roll damping uses vectoring actuators – rudders, azimuthing thrusters, or Voith-Schneider propellers – to generate anti-roll moments without dedicated stabilizers. Since these actuators also control heading and position, this approach requires balancing steering and roll damping (Perez, 2006; Kapitanyuk et al., 2020). Nonminimum-phase roll dynamics limit closed-loop performance (Goodwin et al., 2000), and using actuators at roll frequency increases wear and shortens lifespan. Therefore, dedicated roll stabilizers are generally favored over rudder-based roll damping. These solutions span from passive and semi-passive devices – bilge keels, anti-roll tanks, and fixed or variable-geometry fins – to fully active systems, such as hydraulic or electric fin stabilizers and gyroscopic units, which leverage sensors and advanced control algorithms for optimal roll reduction at the expense of greater complexity.

At cruising speeds and in heavy roll, fin stabilizers typically outperform gyros as they avoid saturation, use less power per torque, and save space. But traditional fins lose effectiveness at low speeds, as lift drops with the square of vessel speed. Zero-speed (flapping) fins overcome this by actively flapping to generate drag-based forces, enabling roll damping even when stationary, mimicking fish fins or bird wings. Research increasingly focuses on modeling low-speed fin hydrodynamics, optimizing fin geometry, and designing advanced control algorithms to improve performance (Liang et al., 2018; Zhang et al., 2019; Song et al., 2019, 2020b; Wei and Yang, 2021; Xu et al., 2025).

This paper presents control and identification methods for a roll-stabilization system with two zero-speed fins, developed by Navis JSC in collaboration with shipbuilders. The proposed algorithms explicitly account for nonlinear drag forces and impose constraints on fin angle and rate due to hydraulic actuator limits. These nonlinearities lead to non-convex optimization problems, typically tackled using robust MPC frameworks (Malekizade et al., 2016) or heuristics like genetic algorithms (Song et al., 2020a).

To enable deployment on low-cost microcontrollers and adaptation to changing sea states, we aim to keep the design simple and within linear control strategies. We study a class of linear controllers and prove robust closed-loop stability under bounded disturbances using the circle criterion for incremental stability (contraction) (D'Alto and Corless, 2013). This stability analysis accounts for nonlinear rate–moment behavior and fin rate saturation. Despite its simplicity, the controller can be tuned to balance global stability and roll damping across sea conditions.

2. MATHEMATICAL MODELLING

Vessel Roll Dynamics. In the standard coordinate system (Fig. 1), the roll dynamics are written as follows

$$J_{xx}\ddot{\theta} + f_d(\dot{\theta}) + mgl(\theta) = M_w(t) + M_u(t). \quad (1)$$

The wave-induced disturbance moment $M_w(t)$ is counteracted by the control moment $M_u(t)$, requiring actuators with sufficient speed and power; J_{xx} is the roll moment of inertia (including added mass), and $mgl(\theta)$ is the restoring moment. The nonlinear roll-damping moment $f_d(\dot{\theta})$ is commonly modeled (Song et al., 2019) as

$$f_d(\dot{\theta}) = 2N_1\dot{\theta} + N_2|\dot{\theta}|\dot{\theta}, \quad (2)$$

[1] Email: {n.savin,e.ambrosovskaya,d.romaev}@navis.spb.ru, anton.p.1982@ieee.org. Please note that some technical details have been omitted here and are available in the extended version of this work, published online on arXiv under the same title.

10.1016/j.ifacol.2025.11.729

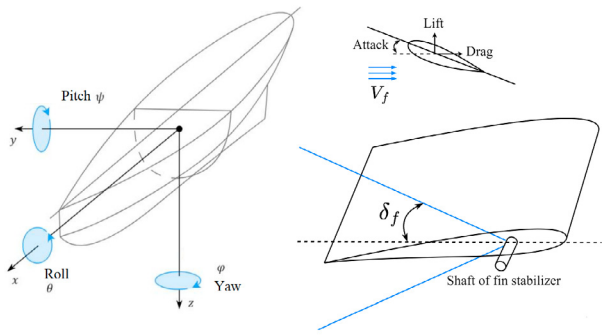

Fig. 1. The ship coordinate system, fin stabilizer angle δ_f

where hydrodynamic coefficients N_1, N_2 depend on vessel speed V and typically increase with V.

For control design, the righting arm $l(\theta)$ and damping moment $f_d(\dot{\theta})$ are linearized: (a) for small roll angles, $l(\theta) \approx h_\theta\,\theta$, where h_θ is the transverse metacentric height; (b) $f_d(\dot{\theta}) \approx N_\theta\,\dot{\theta}$, where N_θ depends on the vessel speed, the amplitude and frequency of roll motion [2]. With these simplifications, the roll dynamics reduce to a linear pendulum equation driven by the inputs $M_w(t)$ and $M_u(t)$:

$$\ddot{\theta} + 2\nu_\theta\omega_0\dot{\theta} + \omega_0^2\theta = \frac{1}{J_{xx}}(M_u(t) + M_w(t)). \tag{3}$$

The natural roll frequency ω_0, the (dimensionless) damping coefficient, and the roll natural period are defined by

$$\omega_0^2 = \tfrac{mg\,h_\theta}{J_{xx}}, \quad \nu_\theta = \tfrac{N_\theta}{J_{xx}\omega_0}, \quad T_0 = \tfrac{2\pi}{\omega_0}.$$

Zero-speed fin stabilizers. For fin stabilizers, the control moment $M_u(t)$ has two components: a lift-based term depending on inflow velocity V_f and fin angle δ_f, and a zero-speed drag term depending only on fin angular rate $\dot{\delta}_f$ (Zhang et al., 2019). Thus, the total control moment is:

$$\begin{gathered} M_u(t) = M_{\text{lift}}(t) + M_{\text{zero}}(t) \\ M_{\text{lift}} = \frac{\rho V_f^2}{2} S_f l_f C_f(\delta_f), \quad M_{\text{zero}} = l_f S_f C_{f0}(\dot{\delta}_f). \end{gathered} \tag{4}$$

Here, ρ is the fluid density, S_f the fin area, l_f the lever arm to the fin's center of pressure, C_f the lift coefficient (dependent on fin profile) (Perez and Blanke, 2012), and C_{f0} the zero-speed force coefficient approximated as [3]

$$\begin{aligned} C_f(\delta_f) &\approx C^\delta \delta_f, \quad C^\delta > 0, \\ C_{f0}(\dot{\delta}_f) &\approx k\dot{\delta}_f|\dot{\delta}_f|, \quad k > 0. \end{aligned}$$

The constants C^δ and k are determined experimentally.

Actuation Dynamics. Fin stabilizers typically use electrohydraulic actuators with full-follow-up (FFU) control (Fig. 2), implemented either in the actuator's inner loop or integrated into the ship's anti-roll system. The two symmetric fins operate synchronously in anti-phase (one deflects up as the other deflects down). Letting $u(t)$

[2] This can be proven by applying the describing-function method (Song et al., 2019; Chechurin and Chechurin, 2017) to (2).

[3] In practice, both fin angle and angular rate are constrained, so the zero-speed coefficient $C_{f0}(\dot{\delta}_f)$ is replaced by a more realistic nonlinear function $h(\dot{\delta}_f)$ to be introduced later. For the operational range of fin angles (ensuring the absence of dynamic stall), the lift force C_f is conventionally approximated as linear.

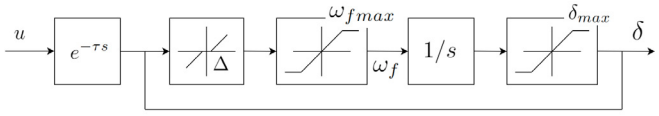

Fig. 2. Fin stabilizer actuator with FFU control.

denote the commanded fin angle, the fin's electrohydraulic actuator obeys the nonlinear equation

$$\omega_f = \dot{\delta}_f = f(u(t-\tau), \delta_f), \tag{5}$$

which is characterized by: (1) transport delay τ; (2) the servo-valve deadband width Δ; (3) maximum fin angular rate, $\omega_{f\,\max}$; (4) maximum fin deflection angle, $\delta_{f\,\max}$; (5) full-stroke travel time (minimum to maximum angle). This nonlinear actuator model is implemented in the vessel-control digital twin (Section 4) and was employed, in particular, for the HIL testing of the anti-roll controller.

For control design, the actuator dynamics (5) are often simplified to the first-order model (Malekizade et al., 2016)

$$\dot{\delta}_f(t) = \frac{u(t) - \delta_f(t)}{T_\delta}, \tag{6}$$

where $T_\delta > 0$ captures the delay and dead-zone effects.

Wave disturbance. Sea-surface elevation is modeled as a stochastic process with spectral density $S(\omega)$, capturing wind-wave energy distribution. The Pierson–Moskowitz and JONSWAP spectra are commonly used. Realizations can be closely approximated by a polyharmonic signal with sufficiently large N, matching $S(\omega)$ in amplitude and frequency, and random phases uniformly distributed over $[0, 2\pi]$ (Perez, 2006, Section 2.10). Thus, we model the wave disturbance moment $M_w(t)$ as a polyharmonic signal:

$$M_w(t) = mgh_\theta\theta_e(t), \quad \theta_e(t) = \sum\nolimits_{i=1}^{N} b_i \sin(\omega_i t + \varphi_i).$$

For each harmonic component i, b_i denotes the amplitude of the effective sea–slope angle; $\omega_i = 2\pi/T_i$ the angular frequency (with T_i the period); and φ_i the phase.

3. CONTROLLER DESIGN

Conventional fin-based roll stabilization typically uses linear control – PID, loop-shaping, H_∞ etc. – enabled by the "quasi-linear" structure of system (3), where damping is linearized and nonlinear drag is often neglected, being dominated by the lift force (see Fig. 6 below). This linearity also supports efficient optimization-based methods that handle actuator constraints, mitigate dynamic stall (Perez and Goodwin, 2008; Jimoh et al., 2021), and use invariant-set techniques (Ghaemi et al., 2009).

In low-speed mode, roll-damping control must leverage the dominant nonlinear drag moment while respecting actuator limits – maximum fin angle and slew rate set by servo-valve dynamics. Control is indirect: although drag depends on fin rate $\omega_f = \dot{\delta}_f$, the commanded input is the fin angle δ_f. This makes optimization-based methods challenging, leading to *non-convex* problems. Existing solutions include robust model-predictive control requiring real-time semidefinite programming (Malekizade et al., 2016), genetic algorithms (Song et al., 2020a), and hybrid fuzzy–sliding-mode schemes (Su et al., 2018).

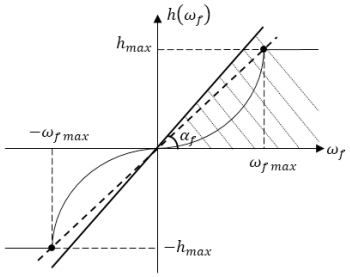

Fig. 3. Saturated zero-speed fins rate-moment curve

The Proposed Controller. For implementation on low-capacity microcontrollers, we use a linear control law:

$$u(t) = (1 - T_\delta c)\delta_f(t) - T_\delta(k_p\theta(t) + k_d\dot{\theta}(t)), \qquad (7)$$

where T_δ is the time constant from (6), and $c > 0$, k_p, k_d are tunable gains. These coefficients must satisfy the circle criterion (see below), ensuring incremental stability of the closed-loop system under any bounded disturbance.

The controller design is motivated as follows. Using the simplified actuator model (6), the fin angle evolves as:

$$\dot{\delta}_f(t) + c\delta_f(t) = \omega_f^*(t) := -k_p\theta(t) - k_d\dot{\theta}(t) \qquad (8)$$

Here, ω_f^* can be seen as the desired fin angular rate. If $c = 0$ and neither δ_f nor $\dot{\delta}_f$ is saturated, then $\dot{\delta}_f = \omega_f^*$. A positive c adds damping to δ_f, stabilizing its dynamics, improving robustness, and helping to avoid saturation.

Accounting for Nonlinearities. In spite of linear controller (8), the vessel-fin-actuator system exhibits nonlinearities. The main nonlinearity is in the control moment, which reduces at low speeds (where M_{lift} is negligible) to:

$$m_u(t) := \frac{1}{J_{xx}}M_u(t) \approx k_{02}\omega_f(t)|\omega_f(t)|, \qquad (9)$$

where $k_{02} > 0$ is constant. Additional nonlinearities stem from the constrained fin angle and angular rate (Fig. 2).

Analyzing systems with multiple nonlinearities is complex, so we apply a standard engineering simplification. The moment in (9) can only be generated for $\omega_f \in [-\omega_{f,\max}, \omega_{f,\max}]$ and saturates at

$$h_{\max} := k_{02}\omega_{f\,\max}^2$$

(or $-h_{\max}$) outside this range. Let $h(\omega_f)$ denote the saturated moment [4]; see Fig. 3. As shown below, the exact rate-torque curve shape is unimportant – only its boundedness and the following *slope restriction* matter:

$$0 \le \frac{h(\omega_1) - h(\omega_2)}{\omega_1 - \omega_2} \le k_f := 2k_{02}\omega_{f\,\max} = \frac{h_{\max}}{\omega_{f\,\max}}. \qquad (10)$$

Under these assumptions, the closed-loop dynamics are:

$$\begin{aligned} \ddot{\theta} + 2n_\theta\dot{\theta} + \omega_0^2\theta &= h(\dot{\delta}_f) + m_w(t), \\ \dot{\delta}_f(t) + c\delta_f(t) &= -k_p\theta(t) - k_d\dot{\theta}(t). \end{aligned} \qquad (11)$$

where $h(\omega_f)$ is the saturated drag-induced control moment and $m_w(t)$ the disturbance moment, both scaled by $1/J_{xx}$. System (11), whose structure is shown in Fig. 4, is a Lur'e

[4] The control torque saturation ensures θ and $\dot{\theta}$ remain bounded for any bounded disturbance $M_w(t)$ due to (3). In practice, choosing small enough gains k_p, k_d and damping $c > 0$ prevents fin angle δ_f and rate $\dot{\delta}_f$ from saturating under controller (7).

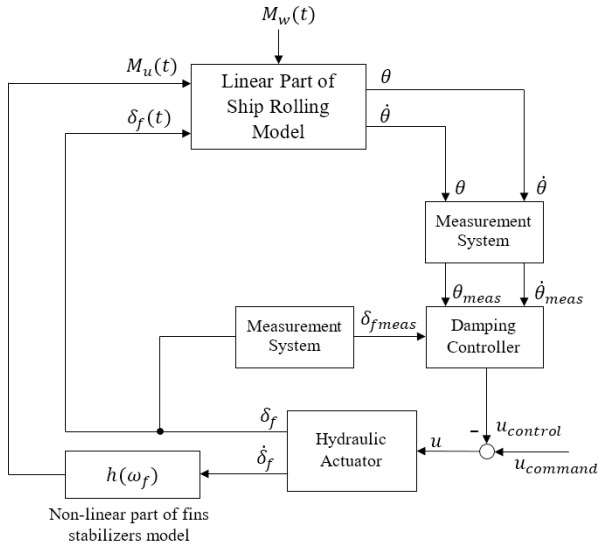

Fig. 4. Plant in Lurie form

system with a scalar nonlinearity $h(\cdot)$ satisfying the slope constraint (10), and subject to external disturbance $m_w(t)$.

Incremental Stability. While bounded $m_w(t)$ ensures bounded solutions, this is a weak form of stability. A stronger and more meaningful property for disturbed systems is Demidovich's "convergent dynamics" (Pavlov et al., 2004), now called *incremental stability* (D'Alto and Corless, 2013) or (strong) *contraction* (Bullo, 2024).

For a general Lur'e-type system with input $w(t)$

$$\dot{x}(t) = Ax(t) + B_h h(y(t)) + B_w w(t), \quad y(t) = Cx(t), \qquad (12)$$

contraction is usually proven using a quadratic Lyapunov function (Pavlov et al., 2004) $V(\Delta x) = (\Delta x)^\top P\Delta x$.

Here, $\Delta x(t) = x(t) - \tilde{x}(t)$ is the difference between two solutions under the same disturbance $w(t)$, and $P = P^\top > 0$ is a positive definite matrix. Under suitable conditions, there exists a P – dependent only on the linear system, not on the nonlinearity or $w(t)$ – such that

$$\frac{d}{dt}V(\Delta x(t)) \le -\varepsilon V(\Delta x(t)), \qquad (13)$$

ensuring exponential decay of the solution difference.

We consider the case where y is scalar and h obeys (10). Denoting the transfer function from h to y as

$$W(s) = C(sI - A)^{-1}B,$$

the following criterion [5] for incremental stability applies (D'Alto and Corless, 2013).

Lemma 1. Assume that A is a Hurwitz [6] matrix and that the following frequency-domain condition holds

$$Re\, W(j\omega) < \tfrac{1}{k_f} \quad \forall\omega \in \mathbb{R}.$$

Then, the Lur'e system (12) is incrementally stable for any nonlinear function h satisfying the slope condition (10). Moreover, there exists a quadratic incremental Lyapunov function $V(\Delta x) = (\Delta x)^\top P\Delta x$ that satisfies (13) for every two solutions $x(t), \tilde{x}(t)$, corresponding to the same

[5] Notice that for a *linear* function $h(y) = ky$, condition (13) reduces to standard stability, so the criterion from Lemma 1 strengthens the classical Nyquist test, ensuring stability for all gains $k \in [0, k_f]$.

[6] A matrix is Hurwitz if all its eigenvalues have negative real parts.

disturbance $w(t)$. Here both $P = P^\top > 0$ and ε depend only on (A, B, C) and k_f, but not on $h(\cdot)$ or $w(t)$.

The incremental stability (13) is important, since it guarantees a number of important properties (Bullo, 2024):

- In the absence of disturbances ($w(t) = 0$), the system admits a unique and exponentially stable equilibrium. If $h(0) = 0$, then the origin $x = 0$ is this equilibrium.
- If $w(t)$ is periodic, then all solutions $x(t)$ converge exponentially fast to a unique forced periodic solution of the same frequency. [7]
- The solution $x(t)$ depends continuously on the disturbance $w(t)$: there exist $C_1, C_2 > 0$ such that [8]
$$\|\Delta x(t)\| \le C_1 e^{-\varepsilon t}\|\Delta x(0)\| + C_2 \sup_{s\in[0,t]} \|\Delta w(s)\|$$
for any two state trajectories $x(t)$ and $\tilde{x}(t)$ corresponding to disturbances $w(t)$ and $\tilde{w}(t)$, respectively. As usual, $\Delta x = x - \tilde{x}$ and $\Delta w = w - \tilde{w}$.
- In particular, if $h(0) = 0$, then applying the previous inequality to $\tilde{x} = 0$ and $\tilde{w} = 0$, one proves that
$$\|x(t)\| \le C_1 e^{-\varepsilon t}\|x(0)\| + C_2 \sup_{s\in[0,t]} \|w(s)\|.$$

By noticing that the transfer function from h to $\omega_f = \dot{\delta}_f$ for the system (11) is found as

$$W(s) = -\frac{s}{s+c}\frac{k_d s + k_p}{s^2 + 2n_\theta s + \omega_0^2},$$

as a corollary of Lemma 1, we obtain the following.

Corollary 2. The system (11) is incrementally stable if h satisfies the slope constraint (10) and

$$Re\,\tilde{W}(j\omega) + \tfrac{1}{k_f} > 0,$$
$$\tilde{W}(j\omega) := -W(j\omega) = \frac{j\omega(k_d j\omega + k_p)}{(j\omega + c)\,(2n_\theta j\omega + \omega_0^2 - \omega^2)}. \quad (14)$$

The frequency-domain conditions for incremental stability can be replaced by LMIs (D'Alto and Corless, 2013; Bullo, 2024), which are convenient when Lur'e system coefficients are fixed. However, if control gains are variables, the LMIs become nonconvex bilinear constraints. In contrast, fixing $c > 0$ makes the left-hand side of (14) linear in (k_d, k_p), so the set of gain pairs satisfying (14) remains convex.

Remarks on The Gain Tuning. The frequency-domain condition can always be met by choosing k_p, k_d sufficiently small – unsurprising, as weak control cannot destabilize an already stable system. However, weak input also fails to damp roll effectively. Thus, selecting gains requires solving an optimization problem that balances nonlinear stability and roll damping – beyond this paper's scope and part of ongoing research. Still, experiments with a realistic vessel model under various sea conditions (see next section) show that gains can be tuned to: (i) achieve satisfactory damping for polyharmonic wave disturbances; (ii) avoid fin angle and rate saturation; and (iii) satisfy the incremental stability condition.

As a first step, we apply harmonic linearization: the system is driven by a sinusoidal input (amplitude and period from slow-averaged disturbance), the equivalent gain is computed, and control gains are chosen to place the linearized poles appropriately [9]. If (14) is violated, k_p and k_d are scaled down until the Nyquist plot of $\tilde{W}(j\omega)$ lies right of $\mathrm{Re} = -\frac{1}{k_f}$. The parameter $c > 0$ minimally affects (14) but helps avoid fin-angle saturation.

[7] This property was first established by Yakubovich (1964).

[8] Constants C_1, C_2 can be found explicitly and depend on P, ε (Bullo, 2024, Theorem 3.16).

4. EXPERIMENTS

This section presents hardware-in-the-loop (HIL) test results for the control algorithm using a realistic ship model, detailed in the next subsection. Vessel performance – with and without roll damping – was evaluated on a testbench (Fig. 5) featuring a digital-twin simulator (Ambrosovskaya, 2014; Ambrosovskaya et al., 2023) with analog/digital interfaces emulating onboard equipment and sensors, including noise and faults. Interfacing the actual roll-damping hardware with the testbench enables evaluation of control and identification algorithms under realistic sampling, latency, and hardware fault conditions (e.g., communication dropouts). Nonlinear characteristics of the electrohydraulic actuators (Fig. 2) – such as valve opening/closing speeds – can also be adjusted. The digital

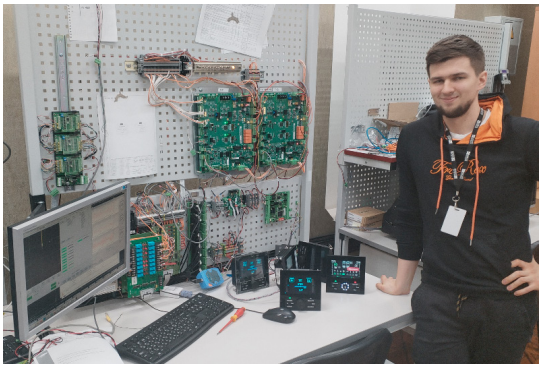

Fig. 5. Testbench (HIL) of roll damping system

twin's motion models support testing under arbitrary noise and disturbance profiles. In the experiments reported below we use a polyharmonic wave model with $N = 10$ harmonics to approximate the Pierson–Moskowitz spectrum for relevant sea states (Chakrabarti, 2005; Perez, 2006).

Ship Principal Characteristic. Key vessel characteristics are summarized in Table 1.

Ship length L, m	49.9
Ship length B, m	9.85
Ship maximum speed V, knt	16
Fin area S, m^2	3
Fin maximal rate ω_{fmax}, deg/s	35
Fin maximal angle δ_{fmax}, deg	60
Actuator time constant T_δ, s	0.14
Transversal metacentric height, m	0.522
Roll natural period at zero speed $T_0 = 2\pi/\omega_0$, s	11

Table 1. Ship particulars

The simulation in Fig. 6 compares lift-based and zero-speed drag components of the control moment (4) at varying vessel speeds. With zero disturbance, the control input is a harmonic fin angle: $u(t) = A_u \sin(\omega_u t)$. Since the drag moment M_{zero} depends nonlinearly on fin rate $\omega_f = \dot{\delta}_f$, it is non-harmonic and phase-shifted relative to the lift-induced moment M_{lift}, which is proportional to

[9] Here advanced methods like LQR or H_∞ control could be used.

δ_f. While M_{zero}'s amplitude stays nearly constant with speed, M_{lift} grows quadratically. Absolute amplitudes also depend on input amplitude ($A_u = 20°$) and period ($T_u = 2\pi/\omega_u = 5\,\text{s}$). Standard fin stabilizers rely on lift forces and are thus effective only above $V_f > 5$ kn.

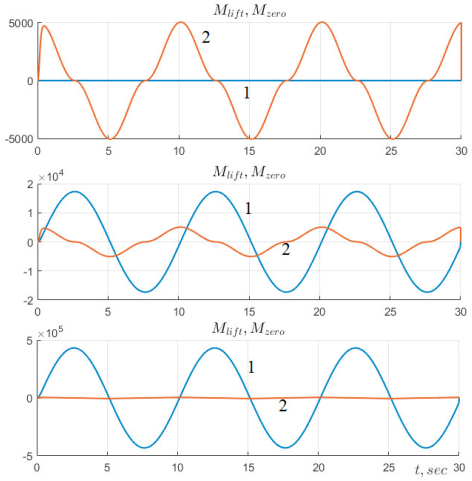

Fig. 6. Fin stabilizers control moments for 0, 3, 15 knots (blue curve 1 – M_{lift}, red curve 2 – M_{zero})

Model identification. The roll-stabilization system supports open-loop mode, allowing direct fin angle commands $u(t)$. Identification maneuvers are conducted in this mode to estimate coefficients in the model

$$\ddot{\theta} = -2n_\theta\dot{\theta} - \omega_0^2\theta + k_1V_f^2\delta_f + k_{02}\dot{\delta}_f|\dot{\delta}_f| \qquad (15)$$

using the standard least-squares method. The equation (15) arises from the roll dynamics (3) by decomposing the control moment into the lifting moment (proportional to $V_f^2\delta_f$) and the drag moment (proportional to $\dot{\delta}_f|\dot{\delta}_f|$).

Since model parameters vary with vessel speed, identification must cover the full operational speed range. In the experiment below, $V_f \approx 0$, so the term $k_1V_f^2\delta_f$ is negligible. We therefore estimate only the natural frequency ω_0, damping coefficient ν_θ, and the fin efficiency k_{02}.

We propose a multi-stage calibration maneuver in which, at each stage, the fin command is a harmonic signal $u(t) = a_i\sin(\omega_i t)$, with stage-specific amplitudes a_i and frequencies ω_i. Between signals of different amplitude, the command is held at zero for a brief interval. Table 3 and Fig. 7 give an example of parameter values; in this example, the maximum period $T_i = 2\pi/\omega_i$ reaches approximately $0.8T_0$, where $T_0 = (2\pi/\omega_0)$ is an apriori estimate of the vessel's natural period from Table 1. Fig. 7 shows the roll response during the calibration maneuver, and the identified coefficients (for the nonlinear model testbench) are listed in Table 2.

	ω_0	ν_θ	k_{01}
Identification	0.729	0.060	0.1188
Model	0.698	0.073	0.1078

Table 2. Identification results

Controlled Roll Dynamics. Finally, we demonstrate the roll response under controller (8) with tuned gains

Stage i	a	$T = 2\pi/\omega$	Duration
1	10	10	$5T$
2	10	8	$5T$
3	10	5	$5T$
4	0	-	30 sec
5	20	10	$5T$
6	20	8	$5T$
7	20	5	$5T$
8	0	-	30 sec

Table 3. Characteristics of the maneuvers

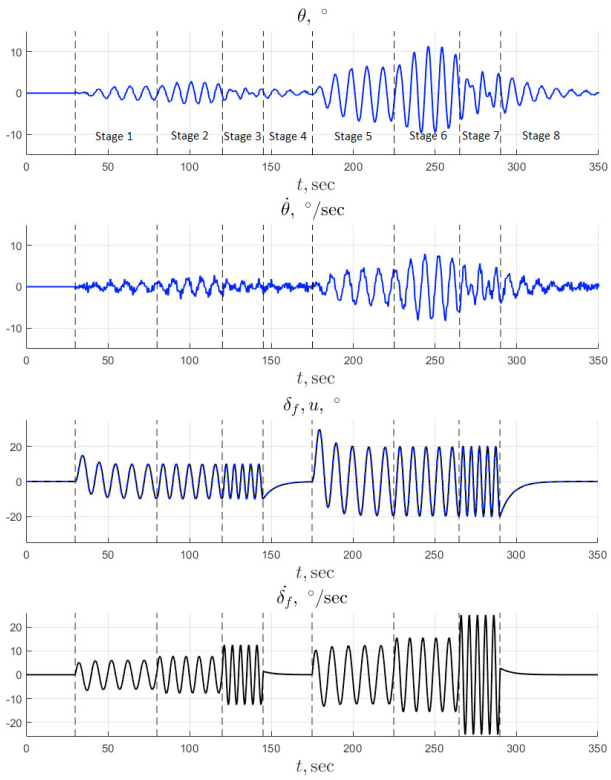

Fig. 7. Roll motion in active identification maneuvers

$k_p = 2.3$, $k_d = 15.1$, and $c = 0.14$. Although the curve $\tilde{W}(j\omega)$ passes close to the critical point $-1/k_f$ (Fig. 8), the frequency-domain condition (14) is still satisfied.

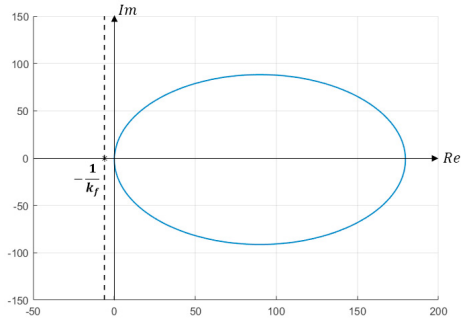

Fig. 8. The Nyquist curve $\tilde{W}(j\omega)$

Fig. 9 illustrates controller effectiveness by comparing roll-model phase portraits with and without control. Once activated, the trajectory converges faster to the phase-plane origin. In these tests, the vessel holds position and heading, with waves incident at 90° from starboard.

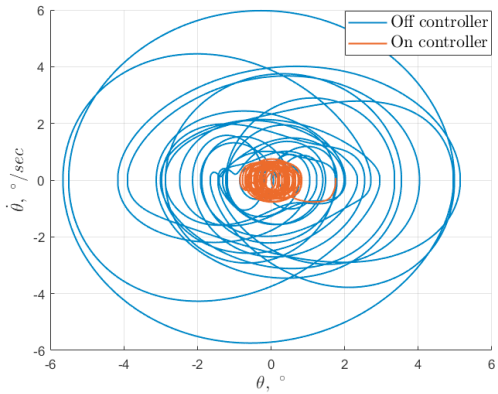

Fig. 9. Phase portrait for wave with sea state code 5 ($H_s = 2.2m$, $T_z = 5.4s$)

CONCLUSION

This paper presented control and identification strategies for a zero-speed fin-based roll stabilization system developed by Navis JSC. We addressed key challenges from the nonlinear drag-induced torque and actuator constraints, proposing a two-stage control scheme that decouples angular rate generation from angle-based inputs to ensure hardware compatibility. While linear control methods are common, we showed that systems with nonlinear rate–torque characteristics require careful stability analysis. Using a frequency-domain contraction criterion, we established conditions for incremental stability. Simulations with a realistic ship model demonstrated the controller's effectiveness in low- and zero-speed roll damping.

This work focuses on low-speed roll damping, which is its primary limitation. A full solution requires tuning both low- and high-speed controllers and implementing bumpless switching logic. Along with a systematic gain selection procedure and experimental validation under varying sea states and loading, this will be addressed in future research. Model identification across different environmental conditions and speeds was not considered here, as experiments were limited to models used in hardware-in-the-loop (HIL) testing.

REFERENCES

Ambrosovskaya, E. (2014). Approach for advanced testing of DP control system. In *MTS DP Conference, Houston*.

Ambrosovskaya, E.B., Ambrosovsky, V.M., and Romaev, D.V. (2023). Mathematical models in ship control systems testbench (in Russian). *Marine Intellectual Technologies*, 89–97.

Bullo, F. (2024). *Contraction Theory for Dynamical Systems*. Kindle Direct Publishing, 1.2 edition. URL `https://fbullo.github.io/ctds`.

Chakrabarti, S.K. (2005). Chapter 3 - ocean environment. In S.K. CHAKRABARTI (ed.), *Handbook of Offshore Engineering*, 79–131. Elsevier.

Chechurin, L. and Chechurin, S. (2017). Nonlinear system oscillations: Harmonic linearization method. In *Physical Fundamentals of Oscillations: Frequency Analysis of Periodic Motion Stability*, 65–81. Springer.

D'Alto, L. and Corless, M. (2013). Incremental quadratic stability. *Numer. Algebra Control Optim.*, 3, 175–201.

Ghaemi, R., Sun, J., and Kolmanovsky, I.V. (2009). Robust control of ship fin stabilizers subject to disturbances and constraints. In *Amer. Contr. Conf.*, 537–542.

Goodwin, G.C., Perez, T., Seron, M., and Tzeng, C.Y. (2000). On fundamental limitations for rudder roll stabilization of ships. In *IEEE Conf. Decision and Control (CDC)*, volume 5, 4705–4710.

Jimoh, I.A., Küçükdemiral, I.B., and Bevan, G. (2021). Fin control for ship roll motion stabilisation based on observer enhanced MPC with disturbance rate compensation. *Ocean Engineering*, 224, 108706.

Kapitanyuk, Y.A., Proskurnikov, A.V., and Cao, M. (2020). Optimal universal controllers for roll stabilization. *Ocean Engineering*, 197, 106911.

Liang, L., Zhao, P., Zhang, S., Ji, M., Jiguang, S., and Yuan, J. (2018). Simulation and experimental study on control strategy of zero-speed fin stabilizer based on disturbance and compensation. *PLoS One*, 13, e0204446.

Malekizade, H., Jahed-Motlagh, M.R., Moaveni, B., Moarefianpour, A., and Ghassemi, H. (2016). Robust model predictive control employed to the container ship roll motion using fin-stabilizer. *Cogent Eng.*, 3, 1235478.

Pavlov, A., Pogromsky, A., Van de Wouw, N., and Nijmeijer, H. (2004). Convergent dynamics, a tribute to Boris Pavlovich Demidovich. *Syst. Contr. Lett.*, 52, 257–261.

Perez, T. (2006). *Ship Motion Control: Course Keeping and Roll Stabilisation Using Rudder and Fins*. Springer.

Perez, T. and Blanke, M. (2012). Ship roll damping control. *Annual Reviews in Control*, 36(1), 129 – 147.

Perez, T. and Goodwin, G.C. (2008). Constrained predictive control of ship fin stabilizers to prevent dynamic stall. *Control Engineering Practice*, 16(4), 482–494.

Song, J., Liang, L., Zhang, S., and Wang, J. (2020a). Design and experimental investigation of a GA-based control strategy for a low-speed fin stabilizer. *Ocean Engineering*, 218, 108234.

Song, J., Zhao, P., Liang, L., and Ji, M. (2020b). Force modeling of zero/low-velocity fin stabilizer and hydrofoil profile optimization. *Ocean Engineering*, 213, 107635.

Song, S., Kim, S.H., and Paik, K.J. (2019). Determination of linear and nonlinear roll damping coefficients of a ship section using CFD. *Brodogradnja*, 70, 17–33.

Su, X., Gao, Y., and Zhao, R. (2018). Roll attitude controller design for ships at zero speed. *International Journal of Fuzzy Systems*, 20, 611–620.

Wei, Y. and Yang, Y. (2021). Research on the hydrodynamic performance of zero speed fin stabilizer. In *International Conference on Offshore Mechanics and Arctic Engineering*, volume Volume 1: Offshore Technology, V001T01A021.

Xu, W., Li, M., Xu, G., Jiao, J., and Liu, H. (2025). Study on the intelligent anti-roll control of a ship at zero speed based on flapping fins. *Ocean Engineering*, 319, 120263.

Yakubovich, V.A. (1964). Method of matrix inequalities in theory of nonlinear control systems stability. I. Forced oscillations absolute stability (in Russian). *Avtomatika i Telemekhanika*, 25(7), 1017–1029.

Zhang, S., You, P., Zhao, P., Liang, L., and Li, R. (2019). Experimental study on the control form of fin stabilizer at zero speed. *PLoS One*, 14, e0216395.